Fe-tourmaline synthesis under different T and f_{O_2} conditions

YVES FUCHS,[1,*] MARTINE LAGACHE,[2] AND JORGE LINARES[3]

[1]Laboratoire de Minéralogie Cristallographie de Paris, URA 09 du CNRS, case 115, Université Pierre et Marie Curie,
4 Place Jussieu, 75252 Paris Cedex 05, France
[2] Laboratoire de Géologie de l'Ecole Normale Supérieure, URA 1316 du CNRS, 24 rue Lhomond, 75005 Paris, France
[3] Laboratoire d'Optique et de Magnétisme, URA 1531 du CNRS, Université de Versailles, 78035 Versailles, France

ABSTRACT

Mössbauer spectrometry of natural samples of tourmaline shows the presence of Fe^{2+} and Fe^{3+} either in the Y (9b) or the Z (18c) sites, with intervalent iron delocalized between these sites. To understand the distribution of iron in natural samples, tourmaline was synthesized at temperatures from 400 to 700 °C, under a pressure of 100 MPa, by the transformation of an Fe^{2+}-rich natural chlorite in the presence of $Na_{0.5}K_{0.5}$-feldspar, boric acid, and H_2O in stoichiometric proportions. The oxygen fugacity, f_{O_2}, of most experiments was buffered by solid assemblages including hematite (HM), nickel-nickel oxide (NNO), and quartz-fayalite-iron (QFI). It was possible to synthesize tourmaline with Fe^{2+} in the Z site and Fe^{2+} or $Fe^{2+} + Fe^{3+}$ in the Y site. These site occupancies are similar to those observed in many natural samples.

For each f_{O_2} buffer, Mössbauer spectrometry shows that Fe^{3+}/Fe^{2+} in the Y site is correlated positively with T and f_{O_2} for $T <550$ °C. For higher temperatures, a negative correlation is observed. These relationships reflect structural changes involving the localization of Fe^{2+} in the Z site and an increasing amount of Al in the Y site. Fe^{3+}/total Fe can be represented by general equations of the type $[\%Fe^{3+}] = e^{(a\ \log f_{O_2} + b)}$. The curves corresponding to each temperature are roughly parallel and equidistant. Thus, Fe tourmaline is a potential geothermometer and an f_{O_2} indicator.

INTRODUCTION

Tourmaline is a common cyclosilicate mineral having the general formula $XY_3Z_6Si_6O_{18}(BO_3)_3(OH)_3(OH,F)$ and the space group $R3m$ (Fig. 1). In the crystallographic notation of Wyckoff (1968), the X, Y, and Z sites of tourmaline correspond to the 3a, 9b, and 18c positions, respectively. The 3a site typically contains large cations like Na, Ca, and to a much lesser extent K, or is partially or totally vacant ($\square$). The octahedral 9b site typically contains Li, Mg, Mn, Fe^{2+}, Fe^{3+}, Ti, and Al, whereas the smaller and less regular octahedral 18c site (Foit 1989) is generally assumed to contain Al, Fe^{3+}, and Mg.

The crystal chemistry of tourmaline is characterized by several solid solutions, with the main types being from the Na-Mg end-member dravite to the Na-Fe^{2+} end-member schorl ($NaMg_3Al_6 \leftrightarrow NaFe_3Al_6$), and from the Na-Li end-member elbaïte to schorl ($NaLi_{1.5}Al_{1.5}Al_6 \leftrightarrow NaFe_3Al_6$). In natural samples, elbaïte-dravite solid solution does not exist. Our analyses of different types of dravite show that their Li contents are normally less than 200 ppm (Paulet 1992; Fuchs and Maury 1995).

Natural tourmalines are generally intermediate solid solutions and show significant compositional variability due to the presence of coupled substitutions. The most common substitutions are alkali deficiency in the X (3a) site, which is charge-balanced by the substitution of R^{2+} by R^{3+} in the Y (9b) site, and proton deficiency, which is charge-compensated by R^{3+} for R^{2+} in the Y (9b) site (Foit and Rosenberg 1977, 1979; Rosenberg and Foit 1985).

Calculations of tourmaline structural formulae are made difficult by the existence of both divalent and trivalent Fe, which are located in both the Y (9b) and Z (18c) sites. However, it is possible to assign sites in tourmaline to Fe^{2+} and Fe^{3+} using Mössbauer spectroscopy (MS). Early studies (Hermon et al. 1973; Mattson and Rossman 1984; Saegusa et al. 1979) assigned Fe^{2+} to the Y (9b) site and Fe^{3+} to the Z (18c) site. Later MS studies revealed the presence of $Fe^{2+} \leftrightarrow Fe^{3+}$ intervalence charge transfer (IVCT) (Burns 1981; Mattson and Rossman 1987a, 1987b). The existence of IVCT phenomena in tourmaline has been also assessed by optical spectroscopy (Faye et al. 1974). The data on site dimensions and ionic radii lead to the assignment of divalent and some trivalent Fe to the Y (9b) site with trivalent Fe substituting for Al in the Z (18c) site, but assignment of the doublet to Fe^{3+} in the Z (18c) site is rare in the MS literature on tourmaline (Gorelikhova et al. 1978; Kovorushkin et al. 1979; Saegusa et al. 1979; Burns 1981; Mattson and Rossman 1984; Ferrow et al. 1988; Fuchs et al. 1995) (Fig. 2).
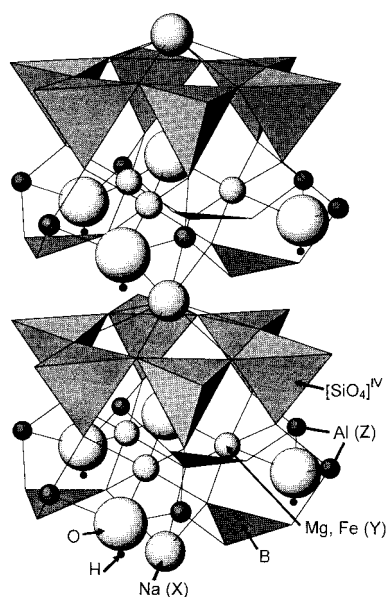
* E-mail: fuchs@ccr.jussieu.fr

FIGURE 1. Structure of Na-Fe, Mg tourmaline, shown parallel to the c axis, drawn with the WATOMS computer program.

Some recent results obtained on natural tourmalines with known chemical composition have shown that Fe^{2+} can be present in the Z (18c) site (Ferrow et al. 1988; Foit et al. 1989; Maury and Fuchs 1991; Fuchs et al. 1995). Some samples show Fe^{2+} in both the Y (9b) and Z (18c) sites, whereas others have only Fe^{2+} in the Z (18c) site and Fe^{2+} and Fe^{3+} in the Y (9b) site. Electron delocalization may take place between the Y (9b) and the Z (18c) sites (Fuchs et al. 1995). The distribution of Fe^{2+} and Fe^{3+} in the Y (9b) and Z (18c) sites is probably affected by f_{O_2} conditions prevailing during the crystallization of tourmaline, or during later
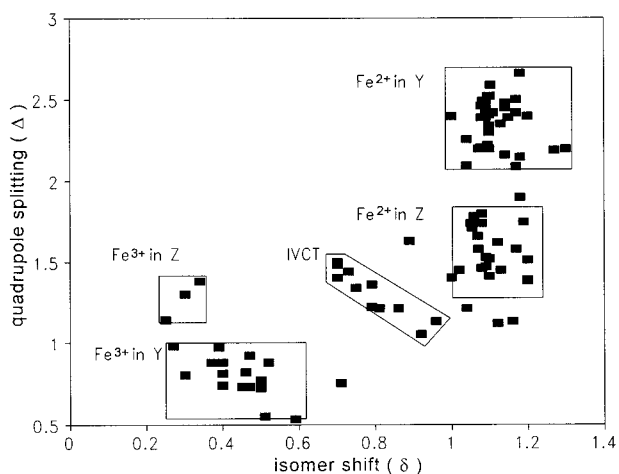

FIGURE 2. Isomer shift (δ) and quadrupole splitting (Δ) values for natural tourmalines (Gorelikhova et al. 1978; Kovorushkin et al. 1979; Saegusa et al. 1979; Burns 1981; Mattson and Rossman 1984; Ferrow et al. 1988; Fuchs et al. 1995).

TABLE 1. ^{37}Fe Mössbauer least-squares fitted parameters (in mm/s), obtained at 300 K, for tourmaline of Uncle Sam Gulch (Montana)
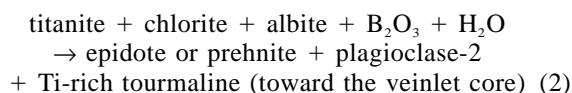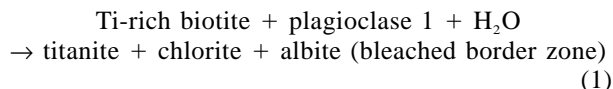
	Attribution	δ	$\Gamma/2$	Δ	% total Fe
1st doublet	Fe^{2+} in Y_1 (9b)	1.087(2)	0.140(6)	2.487(8)	21.4
2nd doublet	Fe^{2+} in Y_2 (9b)	1.087(2)	0.20(4)	1.99(2)	14.9
3rd doublet	Fe^{2+} in Z (18c)	1.035(8)	0.32(2)	1.40(5)	21.1
4th doublet	IVCT	0.52(1)	*0.200*	0.83(3)	8.8
5th doublet	Fe^{3+} in Y (9b)	0.385(3)	*0.200*	0.793(5)	33.9

Notes: The values listed in parentheses correspond to standard deviations. The italic values have been fixed for the fit in order to avoid another mathematical solution.

transformations. Therefore, it is of interest to determine the effect of variable f_{O_2} conditions on the distribution of divalent and trivalent Fe in the octahedral sites of synthetic tourmaline using MS.

SYNTHESIS PROCEDURE

Synthesis procedures were developed based on the observed transformation of biotite to chlorite to tourmaline in natural hydrothermal systems (Fuchs and Maury 1995). For example, at Uncle Sam Gulch near Basin, Montana (Fuchs and Lagache 1994), abundant centimer-scale quartz + tourmaline veinlets, which are developed within a Tertiary granodiorite, show bleached borders. Thin-section observations and electron microprobe analyses reveal that, with the introduction of boron-rich hydrothermal fluids, the following reactions took place:

Ti-rich biotite + plagioclase 1 + H_2O
$\rightarrow$ titanite + chlorite + albite (bleached border zone) (1)

titanite + chlorite + albite + B_2O_3 + H_2O
$\rightarrow$ epidote or prehnite + plagioclase-2
+ Ti-rich tourmaline (toward the veinlet core) (2)

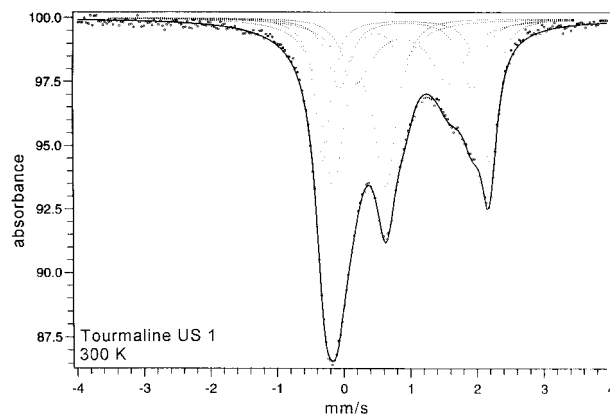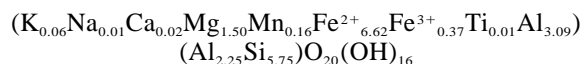MS of this tourmaline US1 (Table 1 and Fig. 3)

FIGURE 3. Mössbauer spectrum of the Uncle Sam Gulch tourmaline (US1) obtained at 300 K.

**TABLE 2.** ^{57}Fe Mössbauer least-squares fitted parameters (as in Table 1) for Monte Fondoli chlorite

	130 K	77 K
δ Fe^{2+}	1.116(1)	1.146
Δ Fe^{2+}	2.885(2)	2.890
$\Gamma/2$	0.24(2)	0.200
% total Fe	93.6	94.3
δ Fe^{3+}	0.28(1)	0.30(2)
Δ Fe^{3+}	0.74(3)	0.87(3)
Γ	0.21(1)	0.200
% total Fe	6.4	5.7

shows 5 doublets corresponding to Fe^{2+} in the Y (9b) site (doublet 1 and 2) and in the Z (18c) site (doublet 3), and to Fe^{3+} in the Y (9b) site (doublet 5). The fourth doublet can be attributed, on the basis of its chemical shift (δ) and quadrupole splitting (Δ), to intervalence charge transfer (IVCT) between Fe^{2+} and Fe^{3+} or to metal-metal charge-transfer (MMCT) between Fe^{2+} and Ti^{4+}.

To synthesize tourmaline in a system approaching natural conditions, an Fe-rich chlorite from the Monte Fondoli deposit (Italy) was selected. It has been verified by X-ray diffraction (XRD) as a 14 Å chlorite, rather than berthierine, in spite of its Fe-rich composition (Slack et al. 1992). Its Mössbauer spectrum (Table 2) shows that the Fe is predominantly divalent (about 95% of the total Fe). Based on assumed oxygen and hydrogen stoichiometry, electron microprobe analyses, and Mössbauer data, the calculated mean structural formula of this chlorite is:

$$(K_{0.06}Na_{0.01}Ca_{0.02}Mg_{1.50}Mn_{0.16}Fe^{2+}_{6.62}Fe^{3+}_{0.37}Ti_{0.01}Al_{3.09})$$
$$(Al_{2.25}Si_{5.75})O_{20}(OH)_{16}$$

The chlorite was sealed into capsules with a gel of $(Na_{0.5}K_{0.5})$-feldspar composition and boric acid. Most of the experiments were carried out under stoichiometric or near-stoichiometric conditions with respect to the following reaction (Fuchs and Lagache 1994):

chlorite + Na, K-feldspar + boric acid
$\rightarrow$ tourmaline + mica + quartz + magnetite $\pm$ H$_2$O
(3)
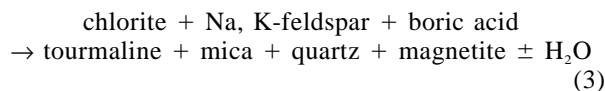
The capsules were heated at T between 400 and 700 °C under a P of 100 MPa. Duration of the experiments depended on temperature and on the type of buffer, and varied from 7 to 142 d. Oxygen fugacity was buffered by the steel alloy of the reaction vessel (VA), and by nickel-nickel oxide (NNO), hematite-magnetite (HM), or quartz-fayalite-iron (QFI) solid assemblages. Reactants were sealed in platinum capsules inserted in a gold capsule containing the solid buffer. The T and f_{O_2} conditions of the experiments, are depicted in Figure 4.

As shown by XRD, reaction 3 was complete at 500, 600, and 700 °C with the formation of muscovite, tourmaline, Fe-oxides, and quartz. Because of the small size of the crystals (1–5 μm width, 10–20 μm length),
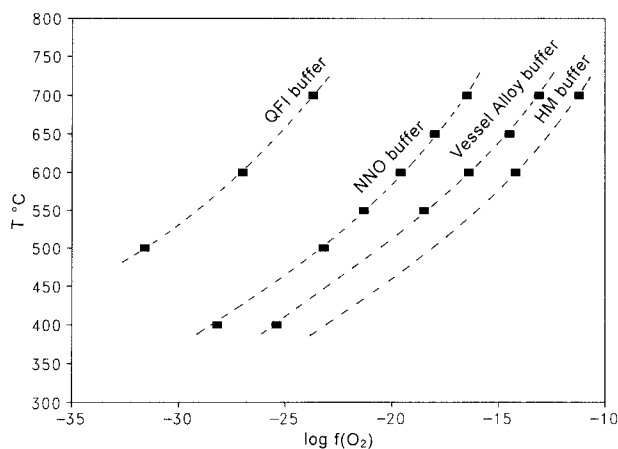

FIGURE 4. Temperature and f_{O_2} conditions (black symbols) used for the experimental synthesis of tourmalines. The curves for the QFI, NNO, and HM buffers are from Eugster and Wones (1962) and the values for the vessel alloy buffer (VA) are from J.L. Robert (personal communication).

however, electron microprobe analyses could not be performed on the synthetic minerals. Semi-quantitative analyses performed with a scanning electron microscope (SEM, see Fig. 5) confirm that the synthesized tourmalines have a largely dominant schorl composition. At 400 °C, reaction 3 occurred but did not go to completion.

RESULTS

Synthetic products obtained in the experiments were identified by XRD and analyzed by MS (Figs. 6–9). Results of the MS are listed in Tables 3a–3e, and summarized in Figure 10. These data can be compared with results reported on natural samples that are shown in Figure 2.

Fe^{2+} and Fe^{3+} are located predominantly in the Y (9b) site in all synthesized tourmalines. The doublets assigned to Fe^{2+} in the Y (9b) site show isomer shifts of $\delta \approx 1.1$ and quadrupole splitting of $\Delta > 2.1$ (Fig. 10). In many cases, particularly for tourmaline synthesized at relatively high T, fit of the spectra is better if two doublets are used for Fe^{2+} in the Y (9b) site. This was also observed for natural samples of tourmaline (Kovorushkin et al. 1979; Fuchs et al. 1995). Kovorushkin et al. (1979) suggested the existence of three non-equivalent Y (9b) sites related to local deformation of the coordination polyhedra due to distribution of cations having different ionic radii.

It seems likely that the better fit obtained by using two different values of Δ reflects only a statistical distribution of trivalent cations (Fe^{3+} or Al) in the neighboring Y (9b) site (Fuchs et al. 1995). The distribution of cations in this site is shown schematically in Figure 11: Fe^{2+} is facing two other divalent cations (Fe^{2+} and/or Mg), as in Figure 11A, two trivalent cations as in 11B, or one divalent and one trivalent cation (Fe^{3+} or
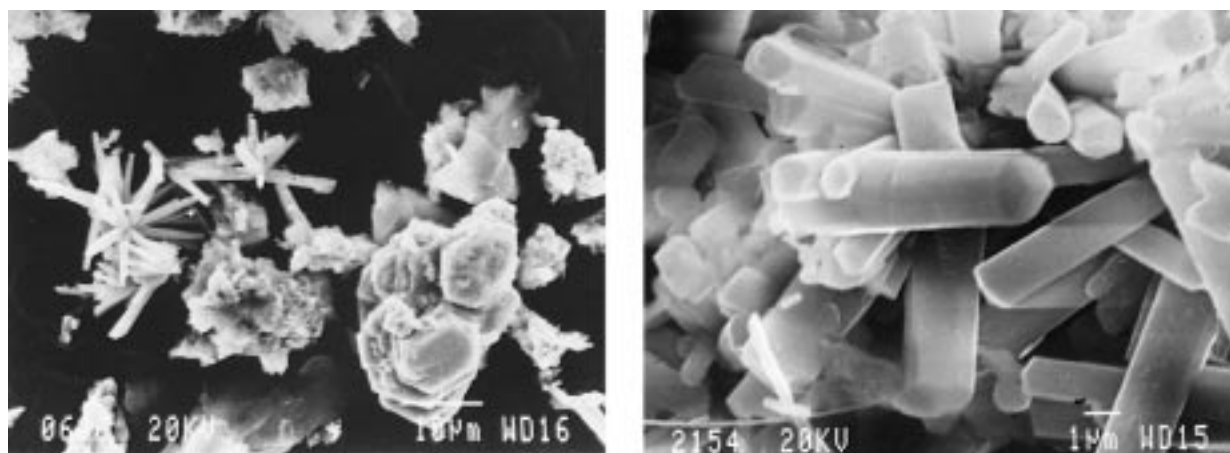
FIGURE 5. SEM images of tourmaline (left) coexisting with mica and (right) automorphous prisms synthesized at 600 °C (experiment B34).

Al), as in 11C. These three distributions appear to represent cases where the Y (9b) site occupancy is 0, ⅓, or ⅔ Fe^{3+}. For example, where the ratio is nearly ½, the structure can be represented either by the statistical distribution of Y (9b) site clusters containing three Fe^{3+} and Y (9b) site clusters with three Fe^{2+} or, alternatively, by ordered or disordered clusters, some with one Fe^{3+} and some with two Fe^{3+} (Fig. 11D). Only in this case would a better fit be obtained by the introduction of two different doublets for Fe^{2+} in the Y (9b) site.

We also attempted to assign doublets with $0.34 \le \delta \le 0.561$ and $0.703 \le \Delta \le 0.96$ (Fig. 10). Although these had been attributed to the Z (18c) site (Linares et al. 1996), a better fit (and comparison with results from the literature, Fig. 2) is obtained if we assign these doublets to Fe^{3+} in the Y (9b) site. In sample B70, the assignment of doublet 4 (Table 3e) is not obvious. The isomer shift value ($\delta = 0.40$) is in good agreement with Fe^{3+} but the quadrupole splitting ($\Delta = 1.130$) can be attributed either to the Y (9b) or Z (18c) sites.

In three cases, a doublet that is characteristic of Fe^{2+} in the Z (18c) site is present: in sample B70 synthesized at 600 °C and $\log f_{O_2} = -27$ (QFI buffer); in B65 synthesized at 700 °C and $\log f_{O_2} = -11.2$ (HM solid buffer); and in B31 synthesized at 700 °C and $\log f_{O_2} = -15.5$ (vessel alloy buffer). Except in experiment B70, no Fe^{3+} or IVCT appears in the Z (18c) site in the synthetic tourmalines, and only a few samples exhibit Fe^{2+} in the Z (18c) site.

The distribution of divalent and trivalent Fe in the Y (9b) and Z (18c) sites, as well as their ratio, depends on the conditions of synthesis. Variations of Fe^{3+} and total Fe are shown as a function of T (Fig. 12) for the tourmalines synthesized under different f_{O_2} buffered conditions. For each buffer the variations are crudely parallel. Fe^{3+} increases slightly with $T \sim 600$ °C in experiments where f_{O_2} was buffered by the vessel alloy, HM, and QFI buffers, and up to ~ 500 °C in experiments buffered by NNO. At higher temperatures, there is a regular decrease in the Fe^{3+} content.
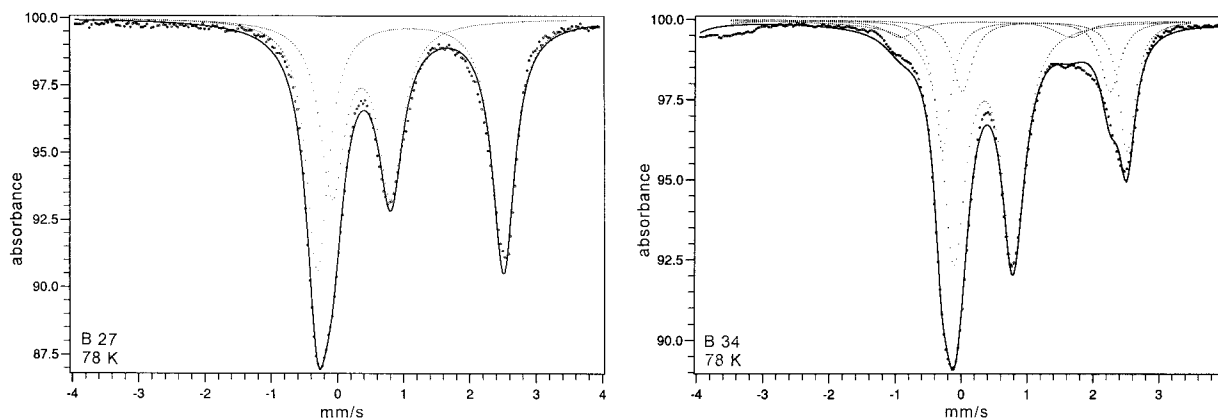

FIGURE 6. Mössbauer spectra obtained at 78 K of tourmalines synthesized in sealed platinum capsules at the f_{O_2} conditions of the VA buffer. Note the differences between the two spectra: (left) B27 (synthesized at 400 °C) shows one doublet for Fe^{2+} in the Y site, (right) whereas B34 (synthesized at 600 °C) shows two doublets indicating the presence of magnetic compound.
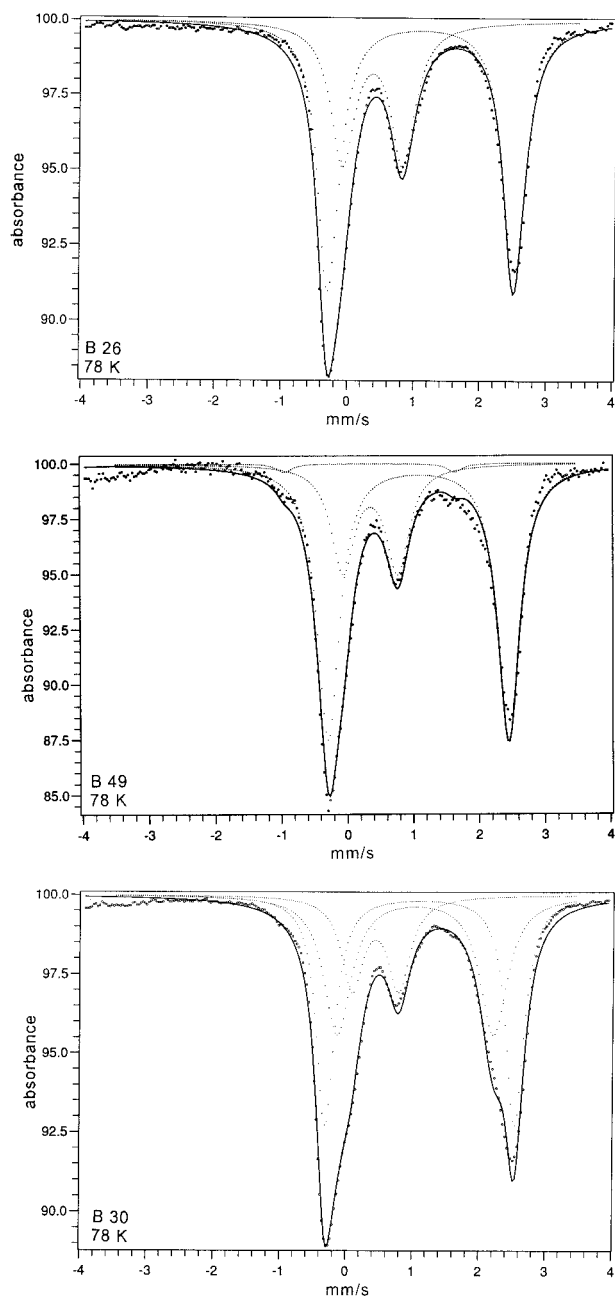
FIGURE 7. Mössbauer spectra obtained at 78 K of tourmalines synthesized at f_{O_2} conditions of the NNO solid buffer. Increasing temperature of synthesis induces changes similar to those of Figure 6 (from top, B26 at 400 °C, B49 at 650 °C, and B30 at 700 °C).

FIGURE 8. Mössbauer spectra obtained at 300 K of tourmalines [B65 (top) at 600 °C and B76 (bottom) at 700 °C] synthesized at f_{O_2} conditions of the HM solid buffer. The two spectra reveal the presence of two different Fe-oxide phases identified on the basis of MS and XRD as hematite and magnetite.

FIGURE 9. Mössbauer spectrum obtained at 300 K of tourmaline B70 synthesized at 600 °C at f_{O_2} conditions of the QFI solid buffer. Note the presence of two Fe^{3+} doublets; one can be attributed to Fe^{3+} in the Y (9b) site, but the attribution of the other remains doubtful.

Variations of Fe^{3+}/total Fe as a function of f_{O_2} are illustrated in Figure 13. For each temperature, there is a positive correlation with log f_{O_2}, and the values of Fe^{3+}/total Fe show a larger increase for the highest values of log f_{O_2}. The curves corresponding to each temperature are roughly parallel and equidistant. These relationships suggest that the ratio of Fe^{3+} in the Y site
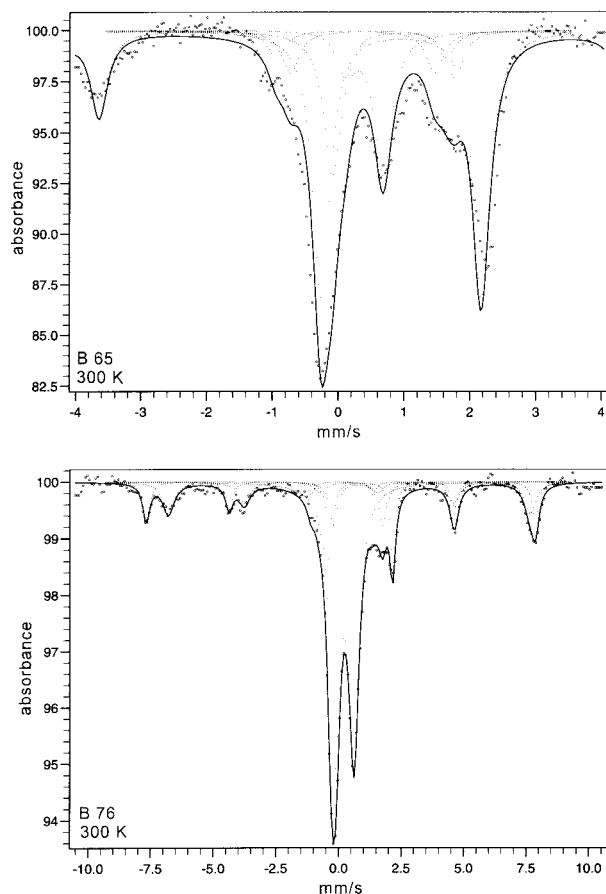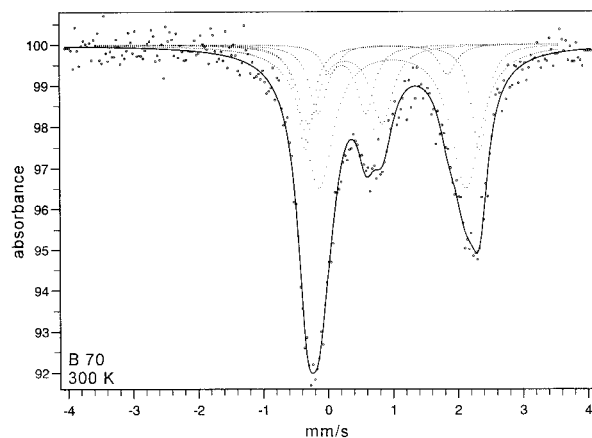
TABLE 3A. Mössbauer fitted parameters (as in Table 1) for tourmaline synthesized at different T in gold-sealed capsules

T	Attribution	B6 500 °C 75 d	B13 600 °C 20 d	B32 600 °C 20 d	B47 700 °C 21 d
δ	Fe^{2+}	1.218(3)	1.207(6)	1.215(3)	1.195(4)
Δ	in	2.753(5)	2.65(1)	2.685(7)	2.679(7)
$\Gamma/2$	Y (9b)	0.228(4)	0.279(9)	0.214(6)	0.209(6)
% total Fe		56.9	52.2	49.1	58.8
δ	Fe^{3+}	0.510(4)	0.475(6)	0.481(4)	0.470(6)
Δ	in	0.848(8)	0.88(1)	0.869(7)	0.86(1)
$\Gamma/2$	Y (9b)	0.238(6)	0.254(7)	0.219(5)	0.216(8)
% total Fe		43.1	47.8	50.9	41.2

to total Fe [$\%Fe^{3+}$] can be represented by a general equation of the type:

$$[\%Fe^{3+}] = e^{(a \log f_{O_2} + b)}$$

Curve fitting was performed for $T = 600$ °C and $T = 700$ °C using least-squares methods. At 600 °C, we obtained the following results (ignoring experiment B70 in which a part of the Fe^3 is not localized precisely; see Table 3e):

$$[\%Fe^{3+}] = e^{(0.144 \log f_{O_2} + 6.41)}$$

and at 700 °C; we obtained:

$$[\%Fe^{3+}] = e^{(0.769 \log f_{O_2} + 4.26)}.$$

In Figure 14, the experimental data are shown as functions of T and $\log f_{O_2}$. The results are distinguished by symbols that correspond to the presence or absence of Fe in the Z (18c) site (filled vs. open squares), and the fitting of Fe^{2+} with one or two doublets in the Y (9b) site (squares with crosses). Data for two natural tourmalines that have only Fe^{2+} in the Y (9b) and Z (18c) sites are also shown. One tourmaline (LH12) is from the Lincoln Hill (Nevada) hydrothermal system

(Paulet 1992), for which T and $\log f_{O_2}$ were calculated using $^{34}S/^{32}S$ of cogenetic sulfides. The Mössbauer data and spectrum for this tourmaline have been published previously (Fuchs et al. 1995). The second tourmaline (EVK) is from a Himalayan granite for which T and $\log f_{O_2}$ were estimated from cogenetic minerals (Table 4). For all samples, the variation of Fe^{3+} in the Y (9b) site, as well as the presence or absence of Fe^{2+} in the Z (18c) site, seem to indicate that structural changes occur in tourmaline that are dependent upon T and f_{O_2}.

On the basis of the MS results obtained on synthetic and natural tourmalines, and on the analyses of natural samples, it appears that three varieties can be distinguished among the schorl groups of Na-Fe-Al tourmalines. The characteristic type (Type 1) forms at low T and relatively high f_{O_2}. It contains all Fe in the Y (9b) site and can be represented by the formula:

$$R^+(Fe^{2+},Fe^{3+})_3Al_6 \text{ etc.}$$
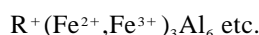
A second intermediate type (Type 2) was found over a wide range of T and f_{O_2} conditions in the experiments. Mössbauer spectra are fitted best by introducing two different subsites for Fe^{2+} in the Y (9b) site. This can be explained by the localization of not only Fe^{3+} but also Al in the Y (9b) site. The presence of R^{3+} cations in the Y (9b) site can be charge-balanced by alkali deficiency in the X (3a) site. This second type can be represented by the formula:

$$\square_x R^+_{1-x} (Fe^{2+},Fe^{3+},Al)_3Al_6 \text{ etc.}$$
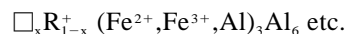
At low T and low f_{O_2}, as well as at high T and high f_{O_2}, a large domain exists where Fe^{2+} is present in the Z (18c) site. This localization of a divalent cation in the Z (18c) site must be charged balanced by a trivalent cation in the Y (9b) site. Al is the most suitable element, and the general composition trends toward the formula:

TABLE 3B. Mössbauer fitted parameters (as in Table 1) for tourmaline synthesized at different T in platinum-sealed capsules with f_{O_2} conditions of the vessel alloy (VA) buffer

T $\log f_{O_2}$	Attribution	B27 400 °C 140 d −25.4	B28 550 °C 22 d −18.5	B34 600 °C 20 d −16.4	B48 650 °C 21 d −14.5	B31 700 °C 20 d −13.2
δ	Fe^{2+}	1.228(2)	1.209(8)	1.230(3)	1.183(3)	*1.221*
Δ	in	2.815(4)	2.65(1)	2.80(1)	2.80(1)	*2.81*
$\Gamma/2$	Y (9b)	0.202(3)	0.21(1)	0.149(7)	0.215(5)	*0.200*
% total Fe		56.9	42.6	24.3	38.9	42.5
δ	Fe^{2+}			1.231(8)	1.21(1)	*1.218*
Δ	in			2.24(2)	2.35(2)	*2.32*
$\Gamma/2$	Y (9b)			0.18(1)	0.20(1)	*0.200*
% total Fe				15.8	18.0	25.1
δ	Fe^{2+}					0.938(2)
Δ	in					1.989(4)
$\Gamma/2$	Z (18c)					0.18(2)
% total Fe						2.8
δ	Fe^{3+}	0.488(3)	0.484(5)	*0.430(3)*	0.50(3)	*0.47*
Δ	in	0.883(6)	0.85(6)	0.893(5)	0.803(8)	*0.917*
$\Gamma/2$	Y (9b)	0.223(4)	0.185(7)	0.204(3)	0.214(6)	*0.200*
% total Fe		43.1	57.4	59.9	43.1	29.6

TABLE 3C. Mössbauer fitted parameters (as in Table 1) for tourmaline synthesized at different T with f_{O_2} conditions of the NNO solid buffer

	Attribution	B26 400 °C 140 d −28.2	B46 500 °C 40 d −23.2	B25 550 °C 22 d −21.3	B33 600 °C 20 d −19.6	B49 650 °C 21 d −18.0	B30 700 °C 20 d −16.5
T							
$\log f_{O_2}$							
δ	Fe^{2+}	1.225(2)	1.127(3)	1.104(2)	1.223(2)	1.204(2)	1.230(2)
Δ	in	2.762(4)	2.59(1)	2.753(4)	2.762(4)	2.742(5)	2.850(5)
Γ/2	Y (9b)	0.40(1)	0.34(2)	0.376(4)	0.41(1)	0.40(1)	0.30(2)
% total Fe		64.5	36.1	60.7	45.5	44.6	42.0
δ	Fe^{2+}		1.14(2)		1.19(2)	1.18(5)	1.164(4)
Δ	in		2.03(8)		2.24(5)	2.32(1)	2.35(2)
Γ/2	Y (9b)		0.56(4)		0.42(1)	0.43(1)	0.50(4)
% total Fe			22.7		19	26.8	38.0
δ	Fe^{3+}	0.484(4)	0.402(9)	0.349(4)	0.468(4)	0.472(7)	0.561(6)
Δ	in	0.908(8)	0.84(2)	0.858(8)	0.862(8)	0.83(1)	0.703(1)
Γ/2	Y (9b)	0.45(1)	0.51(2)	0.41(1)	*0.308*	*0.280*	0.42(4)
% total Fe		35.6	41.2	39.3	35.5	28.6	20.0

$$R^+(Fe_2^{2+}Al)(Fe^{2+}Al_5) \text{ etc.}$$
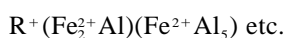
This type (Type 3) was observed in some natural tourmalines from Mount Everest (Visona and Fuchs 1997) and from Nevada (Paulet et al. 1991; Paulet 1992; Fuchs and Maury 1995). However, in natural samples, the total number of Al cations in the Y (9b) site can be >1, depending on alkali deficiency in the X (3a) site that is charge-balanced by the substitution of R^{2+} by R^{3+} in the Y (9b) site and on the existence of significant amounts of Fe^{2+} in the Z (18c) site. The corresponding end-member $\Box(Fe^{2+}Al_2)(Fe^{2+}Al_5)$ etc. has not been observed until now, but natural tourmalines with the formula $\Box_{0.6}Na_{0.4}(Fe_{1.4}^{2+}Al_{1.6})$ $(Fe^{2+}Al_5)$ etc. do occur in some Himalayan granites (Visona and Fuchs 1997).

XRD and MS of the synthetic products show that neither magnetite nor other Fe-oxide minerals are present in products synthesized at $T < 600$ °C (Fig. 15). At 600 °C and higher temperatures, except for the synthe-

sis performed at 700 °C with a QFI solid buffer (B72), Fe oxides are present in the synthetic product because tourmaline does not accept all of the Fe in its structure. For syntheses buffered by the HM solid buffer, two different Fe-oxide phases (magnetite and hematite) are taken into account for the Mössbauer fitting. A positive correlation between the ratio of total Fe present in Fe-oxide phases and $\log f_{O_2}$ is evident for all values of $\log f_{O_2} > -20$ (Fig. 16).

MS has shown that the nature and amount of Fe-oxide phases in the end-products of the syntheses are T and f_{O_2} dependent. This result reinforces our assumption that the structural evolution toward the Type 3 tourmaline implies an increasing role of Al and a de-

TABLE 3D. Mössbauer fitted parameters (as in Table 1) for tourmaline synthesized at different T with f_{O_2} conditions of the HM solid buffer

	Attribution	B76 600 °C 15 d −14.2	B65 700 °C 9 d −11.2
T			
$\log f_{O_2}$			
δ	Fe^{2+}	1.072(7)	*1.077*
Δ	in	2.50(1)	*2.334*
Γ/2	Y (9b)	0.14(1)	*0.160*
% total Fe		13.1	63.9
δ	Fe^{2+}	0.93(4)	
Δ	in	1.97(4)	
Γ/2	Y (9b)	0.20(4)	
% total Fe		10.3	
δ	Fe^+		*1.053*
Δ	in		*1.660*
Γ/2	Z (18c)		*0.160*
% total Fe			10.4
δ	Fe^{3+}	0.480(7)	*0.416*
Δ	in	0.76(1)	*0.773*
Γ/2	Y (9b)	0.247(5)	*0.160*
% total Fe		76.6	25.7

TABLE 3E. Mössbauer fitted parameters (as in Table 1) for tourmaline synthesized at different T with f_{O_2} conditions of the QFI solid buffer

|	Attribution	B71 500 °C 40 d −31.6	B70 600 °C 20 d −27.0	B72 700 °C 8 d −23.7
T				
$\log f_{O_2}$				
δ	Fe^{2+}	1.225(3)	1.108(7)	1.120(4)
Δ	in	2.886(6)	2.68(3)	2.62(2)
Γ/2	Y (9b)	0.220(4)	0.15(3)	0.16(1)
% total Fe		58.8	18.2	20.9
δ	Fe^{2+}	1.276(8)	1.108(7)	1.11(1)
Δ	in	2.15(3)	2.2(1)	2.09(1)
Γ/2	Y (9b)	0.220(4)	0.28(2)	0.228(9)
% total Fe		14.6	45.7	60.5
δ	Fe^{2+}		1.07(3)	1.05(1)
Δ	in		*1.800*	*1.75*
Γ/2	Z (18c)		*0.160*	*0.160*
% total Fe			5.6	7.5
δ	Fe^{3+}		0.40(1)	
Δ	in		*1.130*	
Γ/2	?		*0.200*	
% total Fe			18.1	
δ	Fe^{3+}	0.408(7)	0.34(1)	0.46(6)
Δ	in	0.94(1)	*0.730*	0.8(1)
Γ/2	Y (9b)	0.22(1)	*0.160*	*0.200*
% total Fe		26.6	12.4	11.1
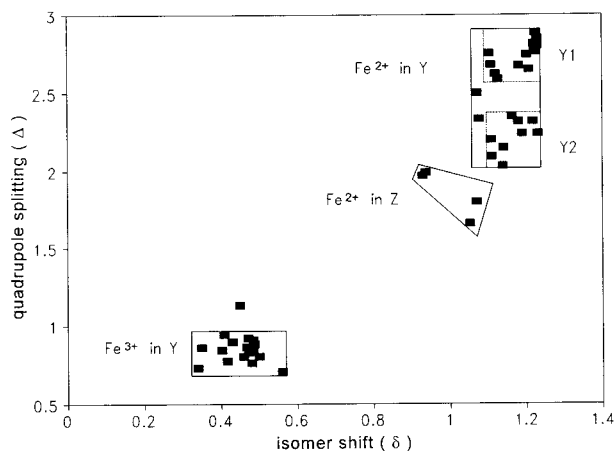
FIGURE 10. Isomer shift (δ) and quadrupole splitting (Δ) values for synthesized tourmalines.

creasing role of Fe in the crystal chemistry of this mineral.

In summary, tourmaline appears to be a good recorder of chemical events during crystallization. Its crystal chemistry, if refined properly using Mössbauer spectrometry, can be very useful for understanding T and f_{O_2} conditions during tourmaline growth. Nevertheless it is necessary to take into account variations that may be induced by post-crystallization oxidation. Moreover, we need to define the conditions that permit tourmaline to contain Fe^{3+} in the Z (18c) site, as reported in some natural samples. These are goals for future experimental studies. Lastly, the present results were all obtained under conditions of stoichiometric
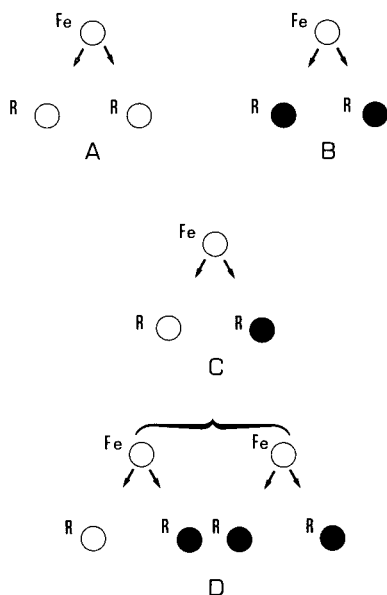
FIGURE 11. Potential distribution and ordering of cations facing Fe^{2+} in the Y (9b) site. Open circles represent divalent Fe and filled circles represent trivalent Fe.
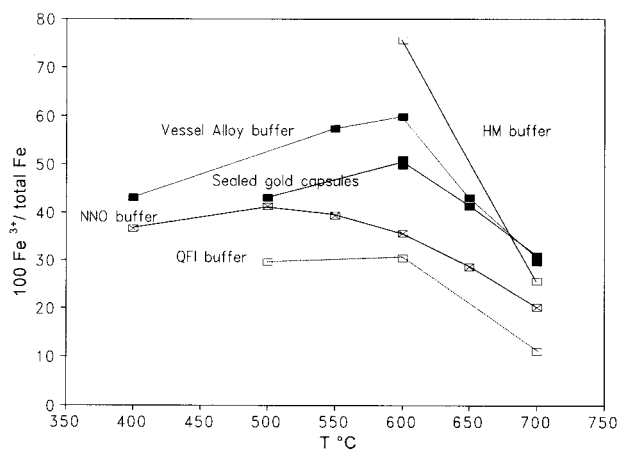

FIGURE 12. A plot of 100 Fe^{3+}/total Fe in tourmalines vs. temperature of synthesis. Each curve corresponds to a different solid buffer, as indicated.
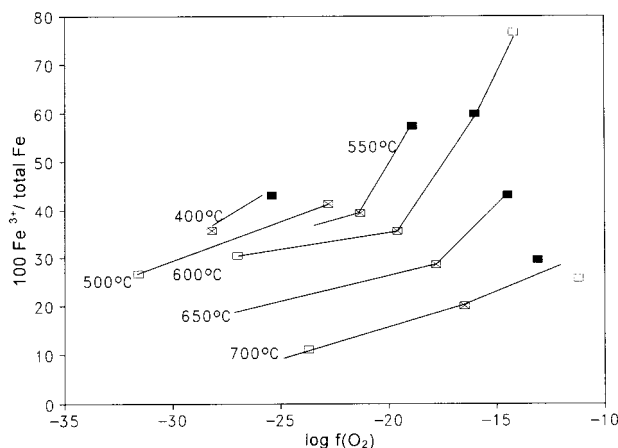

FIGURE 13. A plot of 100 Fe^{3+}/total Fe in tourmalines vs. log f_{O_2} of sepethesis. The curves represent isotherms, as indicated.
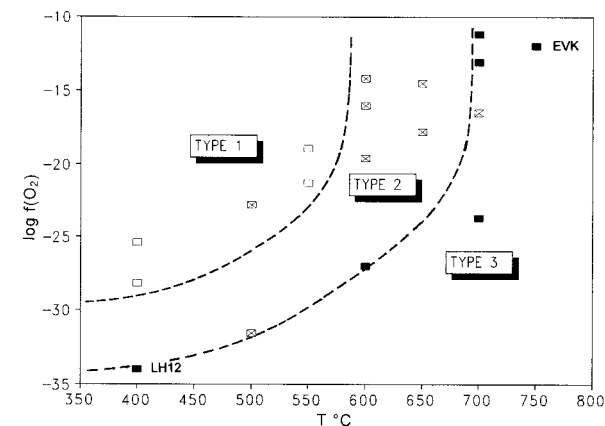

FIGURE 14. Distribution of different types of tourmaline structures in relation to T and log f_{O_2}. LH12 and EVK = natural tourmaline for which T and f_{O_2} parameters can be estimated; filled squares = tourmaline with Fe^{2+} in Z (18c) site; squares with crosses = tourmaline for which Mössbauer spectra are fitted with Fe^{2+} in two Y (9b) sites; open squares = tourmaline for which Mössbauer spectra are fitted with Fe^{2+} in one Y (9b) site.

TABLE 4. Mössbauer fitted parameters (as in Table 1) for natural LH12 and EVK tourmalines at 300 K

Estimated T Estimated log f_{O_2}	Attribution	LH12 400 °C −34	EVK 750 °C −12
δ	Fe^{2+}	1.10(7)	1.100(1)
Δ	in	2.405(2)	2.422(4)
Γ/2	Y (9b)	0.142(2)	0.152(4)
% total Fe		86.5	52.5
δ	Fe^{2+}	1.10(5)	1.056(5)
Δ	in	1.41(1)	1.72(2)
Γ/2	Z (18c)	0.290(2)	0.31(1)
% total Fe		13.5	47.5

proportions of reactions (see Eq. 3). Further experiments now in progress demonstrate that non-stoichiometric conditions, which are common in nature, also influence the distribution of elements in the various sites of tourmaline.
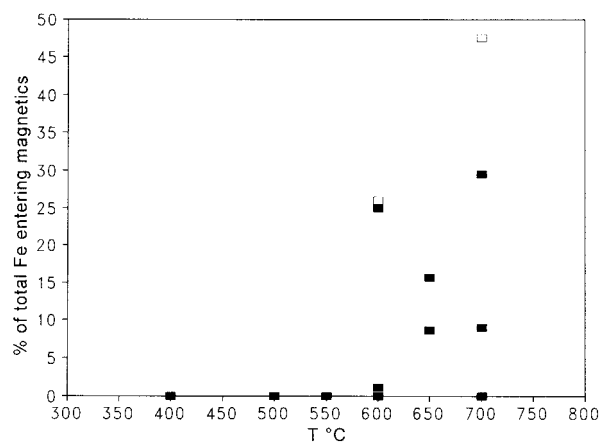
FIGURE 15. Proportion of total Fe entering Fe-oxide phases vs. T °C. Open squares correspond to experiments performed with HM buffer in which two Fe-oxide phases were present.
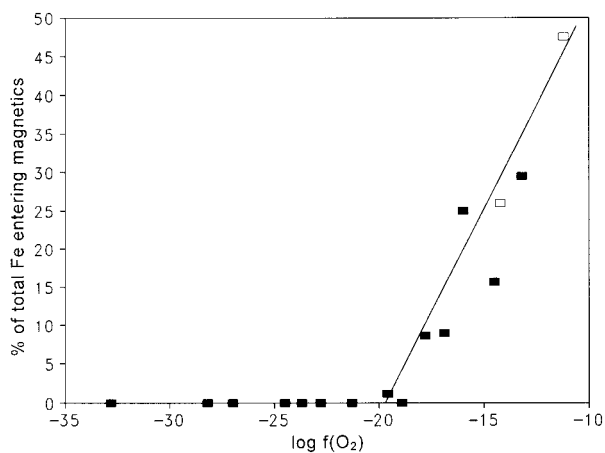
FIGURE 16. Proportion of total Fe entering in Fe-oxide phases vs. log f_{O_2}. Open squares as in Figure 15.

REFERENCES CITED

Burns, R.G. (1981) Intervalence transitions in mixed valence minerals of iron and titanium. Annual Review of Earth and Planetary Sciences, 9, 345–353.

Eugster, H.P. and Wones, D.R. (1962) Stability relations of the ferruginous biotite, annite. Journal of Petrology, 3, 82–125.

Faye, G.H., Manning, P.G., Gosselin, J.R., and Tremblay, J.R. (1974) The optical absorption spectra of tourmaline: Importance of charge-transfer processes. Canadian Mineralogist, 12, 370–380.

Ferrow, E.A., Annersten, H., and Gunardawane, R.P. (1988) Mössbauer effect study on the mixed valence state of iron in tourmaline. Mineralogical Magazine, 52, 221–228.

Foit, F.F., Jr. (1989) Crystal chemistry of alkali-deficient schorl and tourmaline structural relationships. American Mineralogist, 74, 422–431.

Foit, F.F., Jr. and Rosenberg, P.E. (1977) Coupled substitutions in the tourmaline group. Contributions to Mineralogy and Petrology, 62, 109–127.

——— (1979) The structure of vanadium-bearing tourmaline and its implications regarding tourmaline solid solutions. American Mineralogist, 64, 788–798.

Foit, F.F., Jr., Fuchs, Y., and Myers, P.E. (1989) Chemistry of alkali-deficient schorls from two tourmaline-dumortierite deposits. American Mineralogist, 74, 1317–1324.

Fuchs, Y. and Lagache, M. (1994) Les transformations chlorite-tourmaline en milieu hydrothermal, exemples naturels et approche expérimentale. Comptes Rendus à l'Académie des Sciences, Paris, 319 (II), 907–913.

Fuchs, Y. and Maury, R. (1995) Borosilicate alteration associated with U-Mo-Zn and Ag-Au-Zn deposits in volcanic rocks. Mineralium Deposita, 30, 449–459.

Fuchs, Y., Lagache, M., Linares, J., Maury, R., and Varret, F. (1995) Mössbauer and optical spectrometry of selected schorl-dravite tourmalines. Hyperfine Interactions, 96, 245–258.

Gorelikhova, N.V., Perfil'yev, Y.D., and Bubeshkin, A.M. (1978) Mössbauer data on distribution of Fe ions in tourmaline. International Geology Review, 20, 982–990.

Hermon, E., Simkin, D.J., Donnay, G., and Muir, W.B. (1973) The distribution of Fe^{2+} and Fe^{3+} in iron bearing tourmalines: A Mössbauer study. Tschermaks Mineralogische und Petrographische Mitteilungen, 19, 124–132.

Kovorushkin, V.V., Kuzmin, V.I., and Belov, V.F. (1979) Mössbauer studies of structural features of tourmaline of various genesis. Physics and Chemistry of Minerals, 4, 209–220.

Mattson, S.M. and Rossman, G.R. (1984) Ferric iron in tourmaline. Physics and Chemistry of Minerals, 11, 225–234.

——— (1987a) Fe^{2+}-Fe^{3+} interactions in tourmaline. Physics and Chemistry of Minerals, 14, 163–171.

——— (1987b) Identifying characteristics of charge transfer transitions in minerals. Physics and Chemistry of Minerals, 14, 94–99.

Maury, R. and Fuchs, Y. (1991) Tourmalines structural refinement based on Mössbauer spectrometry, EUG VI, Strasbourg, Diffusion and order-disorder kinetics in minerals. Terra Abstract, 23.

Paulet, P.H. (1992) Etude des altérations hydrothermales à borosilicates de la Humboldt Range, Nevada, USA. Thesis, 163 p. Université Pierre et Marie Curie, Paris.

Paulet, P.H., Fuchs, Y., Maury, R., Foit, F.F., Jr., and Rosenberg, P.E. (1991) Zonalité des différents types de borosilicates dans les systèmes hydrothermaux à or-argent de la Humboldt Range (Nevada, U.S.A.). Comptes Rendus à l'Académie des Sciences, Paris, 313(II), 1155–1162.

Rosenberg, P.E. and Foit, F.F., Jr. (1985) Tourmaline solid solutions in

the system MgO-Al_2O_3-SiO_2-B_2O_3-H_2O. American Mineralogist, 70, 1217–1223.

Saegusa, N., Price, D.C., and Smith, G. (1979) Analysis of the Mössbauer spectra of several iron rich tourmalines (schorl). Journal of Physics, Colloque C2, 40, 456–459.

Slack, J.F., Jiang, W.-T., Peacor, D.R., and Okita, P.M. (1992) Hydrothermal and metamorphic berthierine from the Kidd Creek volcanologic massive sulfide deposit, Timmins, Ontario. Canadian Mineralogist, 30, 1127–1142.

Visona, D. and Fuchs, Y. (1997) Dumortierite, a new mineral from Himalayan leucogranites: Petrological implications. Second International Symposium on Granites and Associate Mineralizations, Salvador, Brazil. Extended abstract, 247–248.

Wyckoff, R.G.W. (1968) Crystal Structures, 4, Intersciences, New York.